https://doi.org/10.15407/ujpe71.3.221

J. SENTHIL KUMAR,[1] N. SIVA JYOTHI,[2] S. SUMATHI,[3] N. KARTHIK,[3]
S. JEYAVIJAYAN[3]

[1] PG & Research Department of Physics, Thanthai Periyar Government Arts and Science College
(36/2, Race Course Road, Kajamalai Colony, Tiruchirappalli, Tamil Nadu 620023, India; e-mail: josenthil74@gmail.com)
[2] Department of Physics, Periyar Maniammai Institute of Science and Technology
(Periyar Nagar, Vallam, Tamil Nadu 613403, India; e-mail: sivajyothinatarajan@gmail.com)
[3] Department of Physics, Kalasalingam Academy of Research and Education
(Anand Nagar, Krishnankoil-626126, Tamil Nadu, India; e-mail: sjeyavijayan@gmail.com)

SPECTROSCOPIC ANALYSIS, DFT CALCULATIONS, HIRSHFELD SURFACE AND MOLECULAR DOCKING STUDIES OF 5-CHLORO-1-PHENYL-1H-TETRAZOLE: A POTENTIAL ANTI-BREAST CANCER AGENT

This study presents a comprehensive theoretical and spectroscopic investigation of 5-chloro-1-phenyl-1H-tetrazole (5CPT). The compound was characterized using FT-IR, FT-Raman, X-ray diffraction (XRD), and UV-visible spectroscopy. Quantum chemical calculations were performed at the DFT/B3LYP/6-311++G(d,p) level to support and interpret the experimental findings. The simulated XRD pattern was compared with the experimental data for structural validation. Vibrational frequencies derived from FT-IR and FT-Raman spectra were calculated at the same theoretical level and showed good agreement with the experimental results. Mulliken population analysis and molecular electrostatic potential (MEP) mapping were employed to analyze the electronic distribution and identify reactive sites within the molecule. UV-visible absorption maxima (λ) were determined through both experimental measurements and time-dependent DFT (TD-DFT) calculations. Analysis of Hirshfeld surfaces and fingerprints revealed information about interactions within and between molecules. Furthermore, molecular docking studies against breast cancer-related target proteins revealed binding affinities in the range of –7.0 to –6.6 kcal/mol. ADMET predictions indicated favorable pharmacokinetic and toxicity profiles. Collectively, the docking and ADMET results suggest that 5CPT may serve as a promising candidate for anti-breast cancer drug development.

K e y w o r d s: 5-chloro-1-phenyl-1H-tetrazole, DFT, molecular docking, ADMET, breast cancer.

1. Introduction

Tetrazole derivatives have attracted considerable attention in medicinal chemistry owing to their distinctive structural features, including their ability to mimic carboxylic acid functionalities, strong hydrogen-bonding capacity, and favorable metabolic stability [1, 2]. In oncology research, compounds containing the tetrazole moiety are increasingly investigated for their anticancer potential, particularly due to their capacity to modulate critical cellular pathways involved in tumor growth, survival, and metastasis [3]. 5-chloro-1-phenyl-1H-tetrazole (5CPT) is a heterocyclic compound characterized by a tetrazole ring substituted with a phenyl group at the 1-position and a chlorine atom at the 5-position. The phenyl ring contributes to enhanced hydrophobic interactions with biological targets, while the chlorine substituent alters the electronic distribution of the molecule, potentially increasing its binding affinity

C i t a t i o n: Kumar J. Senthil, Jyothi N. Siva, Sumathi S., Karthik N., Jeyavijayan S. Spectroscopic analysis, DFT calculations, Hirshfeld surface and molecular docking studies of 5-chloro-1-phenyl-1H-tetrazole: a potential anti-breast cancer agent. *Ukr. J. Phys.* **71**, No. 3, 221 (2026). https://doi.org/10.15407/ujpe71.3.221.

and selectivity toward oncogenic proteins such as kinases, proteases, and transcription factors [4]. Moreover, tetrazole rings exhibit strong coordination ability with metal ions and active enzymatic sites, making them valuable scaffolds for the design of kinase inhibitors and apoptosis-inducing agents. The compact and polar nature of 5CPT further supports improved aqueous solubility and bioavailability, which are critical parameters in the drug development process.

Recent research on tetrazole-based compounds has focused on their potential to inhibit angiogenesis, induce cell cycle arrest, and overcome drug resistance key challenges in cancer treatment [5]. In this context, 5CPT and its structural analogs have emerged as promising lead candidates for the development of new anticancer agents. The molecular architecture of 5CPT supports favorable membrane permeability and incorporates functional groups capable of engaging in essential non-covalent interactions, making it a strong contender for pharmacological studies targeting enzymes, bacteria, or cancer cells. While numerous tetrazole derivatives have been investigated using density functional theory (DFT) for their biological and anticancer properties [6], a comprehensive study integrating molecular docking, ADMET analysis, and quantum chemical evaluation of 5CPT has not yet been reported.

In this study, the molecular structure of 5CPT was validated by comparing its simulated X-ray diffraction (XRD) pattern with the corresponding experimental data. Density Functional Theory (DFT) calculations, performed at the B3LYP/6-311++G(d,p) level, were employed to gain comprehensive insights into the molecule's vibrational and electronic properties. The optimized geometry was confirmed by comparing the calculated bond lengths and bond angles with those obtained from experimental XRD analysis. Spectroscopic investigations, including FT-IR, FT-Raman, and UV-Vis analyses, were conducted to characterize the vibrational modes and electronic transitions of the molecule. The electronic structure, particularly the highest occupied molecular orbital (HOMO) and lowest unoccupied molecular orbital (LUMO), was examined using time-dependent DFT (TD-DFT) at the same theoretical level. Furthermore, Mulliken atomic charge analysis and molecular electrostatic potential (MEP) mapping were utilized to visualize charge distribution and identify potential reactive sites. Molecular docking studies were carried out to assess the binding affinity of 5CPT to breast cancer-associated target proteins, and ADMET (absorption, distribution, metabolism, excretion, and toxicity) analysis was performed to evaluate its pharmacokinetic and toxicological characteristics.

2. Experimental Details

For experimental analyses, a 98% pure sample of 5CPT was obtained from Sigma-Aldrich, India, and used without further purification. Powder X-ray diffraction (XRD) was performed using a Bruker D8 Advance ECO diffractometer equipped with an SSD160 one-dimensional (1D) detector and a Cu-Kα radiation source ($\lambda = 1.5406$ Å). Measurements were conducted at room temperature under operating conditions of 40 kV and 25 mA. Data were collected over a 2θ range of 5 to 50 at a scanning rate of 2° per minute. The experimental diffraction pattern exhibited good agreement with the calculated unit cell parameters, including lattice constants and volume. Infrared (IR) spectra were recorded using a Shimadzu IR Tracer-100 spectrometer. The sample was ground, mixed with potassium bromide (KBr), and pressed into a pellet prior to measurement. Spectral data were collected over the wavenumber range of 4000–400 cm^{-1}. The FT-Raman spectrum was obtained using a Bruker RFS 27 standalone FT-Raman spectrometer, covering the same wavenumber range with a spectral resolution of 2 cm^{-1}. Ultraviolet-visible (UV-Vis) absorption spectra were recorded using a U-3501 spectrophotometer across a wavelength range of 100–500 nm.

3. Theoretical Studies

All quantum chemical calculations were performed using the DFT framework implemented in the Gaussian 09W software package [7]. Geometry optimization of the 5CPT molecule was conducted at the B3LYP level with the 6-311++G(d,p) basis set [8, 9]. The optimized molecular structure was visualized using GaussView 05 software [10]. Vibrational wavenumbers were calculated and assigned based on potential energy distribution (PED) analysis using the VEDA program [11]. Time-dependent DFT (TD-DFT) calculations at the same theoretical level were employed to predict the absorption maxima of 5CPT. Additional analyses included Mulliken atomic charge distribution, molecular electrostatic potential (MEP) mapping, and frontier molecular or-

Table 1. **Optimized structural parameters of 5-chloro-1-phenyl-1H-tetrazole**

Structural parameters	DFT-B3LYP/ 6-311++G(d,p)	Experimental [19]
Bond length (Å)		
N1–N2	1.363	1.357
N1–C5	1.355	1.341
N1–C7	1.430	1.439
N2–N3	1.287	1.293
N3–N4	1.358	1.357
N4–C5	1.310	1.309
C5–Cl6	1.708	1.684
C7–C8	1.393	1.373
C7–C12	1.394	1.373
C8–C9	1.392	1.383
C8–H17	1.083	0.930
C9–C10	1.394	1.364
C9–H16	1.084	0.930
C10–C11	1.394	1.373
C10–H15	1.084	0.930
C11–C12	1.392	1.392
C11–H14	1.084	0.930
C12–H13	1.083	0.930
Bond angle (°)		
N2–N1–C5	106.5	107.3
N2–N1–C7	121.5	122.27
C5–N1–C7	131.9	130.44
N1–N2–N3	106.8	106.14
N2–N3–N4	111.6	111.63
N3–N4–C5	105.3	105.02
N1–C5–N4	109.8	109.93
N1–C5–Cl6	124.9	123.75
N4–C5–Cl6	125.3	126.31
N1–C7–C8	120.0	118.32
N1–C7–C12	118.7	119.05
C8–C7–C12	121.3	122.63
C7–C8–C9	119.1	118.51
C7–C8–H17	120.3	120.7
C9–C8–H17	120.6	120.7
C8–C9–C10	120.3	120.20
C8–C9–H16	119.5	119.9
C10–C9–H16	120.2	119.9
C9–C10–C11	120.0	120.57
C9–C10–H15	120.0	119.7
C11–C10–H15	120.0	119.7
C10–C11–C12	120.3	120.52
C10–C11–H14	120.2	119.7
C12–C11–H14	119.5	119.7
C7–C12–C11	119.1	117.56
C7–C12–H13	119.7	121.2
C11–C12–H13	121.2	121.2

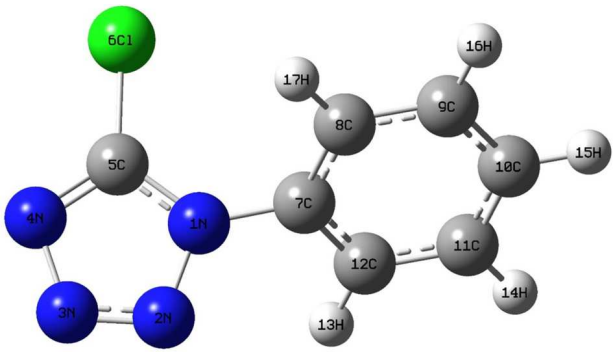

Fig. 1. Optimized structure of 5-chloro-1-phenyl-1H-tetrazole

bital (HOMO–LUMO) evaluation. Simulated single-crystal XRD patterns were generated using the VESTA software package [12]. Using Crystal Explorer 17.5, the fingerprint and Hirshfeld surface were mapped [13]. Molecular docking studies were carried out using AutoDock and PyRx tools [14, 15] to assess the interaction of 5CPT with breast cancer-related target proteins obtained from the Protein Data Bank (PDB). The resulting two-dimensional (2D) and three-dimensional (3D) interaction profiles were visualized and analyzed using Discovery Studio software [16]. The SMILES representation of 5CPT was retrieved from the PubChem database and used to predict ADMET properties via the pkCSM web server [17]. Key pharmacokinetic parameters such as lipophilicity, water solubility, and drug-likeness were evaluated, along with radar plot analyses. Furthermore, gastrointestinal absorption and blood–brain barrier (BBB) permeability were estimated using the SwissADME online tool, incorporating the BOILED-Egg model [18].

4. Results and Discussion

4.1. Molecular geometry

The optimized molecular structure of 5CPT, which belongs to the C_1 point group, is depicted in Fig. 1. The structure was optimized using DFT at the B3LYP/6-311+ +G(d,p) level. A detailed comparison between the experimental crystallographic data and the DFT-optimized geometrical parameters, including bond lengths and bond angles, is provided in Table 1. The molecule consists of a conjugated system incorporating nitrogen–nitrogen (N–N) and carbon–carbon (C–C) bonds, along with a chlorine substituent. Key structural parameters in-

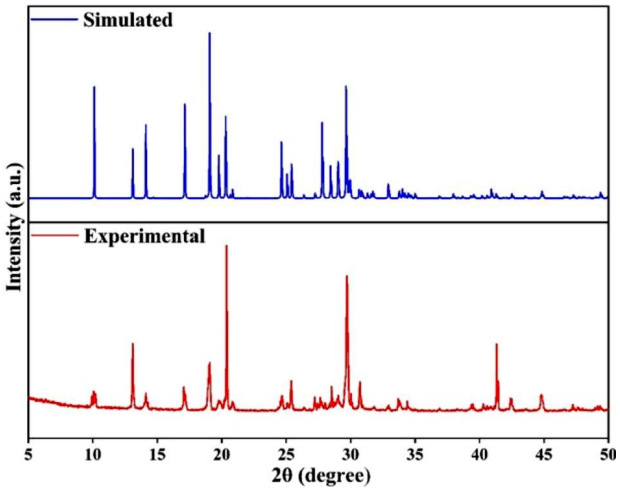

Fig. 2. Simulated and experimental comparison of XRD for 5-chloro-1-phenyl-1H-tetrazole

Table 2. **Thermodynamic parameters of 5-chloro-1-phenyl-1H-tetrazole**

Parameters	DFT-B3LYP/ 6-311++G(d,p)
Optimized global minimum Energy (Hartrees)	–949.03314
Total energy(thermal), E_{total} (kcal mol^{-1})	79.331
Heat capacity, C_v (cal mol^{-1} k^{-1})	33.802
Total Entropy, S (cal mol^{-1} k^{-1})	94.604
Translational Entropy (cal mol^{-1} k^{-1})	41.470
Rotational Entropy (cal mol^{-1} k^{-1})	30.866
Vibrational Entropy (cal mol^{-1} k^{-1})	22.268
Vibrational energy, E_{vib} (kcal mol^{-1})	77.553
Zero-point vibrational energy, (kcal mol^{-1})	73.830
Rotational constants (GHz)	
A	1.570
B	0.653
C	0.476
Dipole moment (Debye)	5.862

volving C–Cl, N–N, N–C, and C–C–H groups were thoroughly examined. Overall, the calculated bond lengths and angles show strong agreement with experimental XRD data [19], with minor discrepancies attributed to the inherent differences between gas-phase theoretical calculations and solid-state experimental measurements. For instance, the calculated C5–Cl6 bond length (1.708 Å) closely matches the experimental value (1.684 Å), while the N1–N2 bond length (1.363 Å) is nearly identical to the experimental result (1.357 Å). The DFT-predicted C–H bond lengths range from 1.083 to 1.084 Å, compared to approximately 0.930 Å observed experimentally [19], which is typical due to X-ray diffraction's known limitations in accurately locating hydrogen positions. Similarly, experimental C–C bond lengths range from 1.364 Å to 1.392 Å, while theoretical values lie between 1.392 Å and 1.394 Å. Theoretical and experimental values for other bonds, such as N2–N3 (1.287 Å vs. 1.293 Å) and N3–N4 (1.358 Å vs. 1.357 Å), further confirm the reliability of the computational model. Bond angles also exhibit excellent consistency; for example, the calculated angle N2–N1–C5 (106.5°) closely approximates the experimental angle (107.3°), with similar alignment observed throughout the molecular structure. To further validate the molecular conformation and crystalline phase, XRD analysis was performed. A comparison of the simulated and experimental XRD patterns is shown in Fig. 2. The simulated pattern, based on the DFT-optimized structure, successfully reproduces the major experimental peaks in both position and intensity. This strong correlation confirms the compound's crystallinity and phase purity, and reinforces the accuracy and structural reliability of the DFT-optimized model.

4.2. Thermodynamic parameters

Statistical mechanics serves as a vital tool for translating molecular energy levels arising from vibrational, rotational, translational, and electronic excitations into macroscopic thermodynamic properties such as entropy and heat capacity [20, 21]. These thermodynamic parameters offer valuable insights into the behavior of molecules within biological systems. Among them, entropy (S) plays a crucial role in evaluating a molecule's binding affinity to its target, as it reflects the inherent tendency of chemical systems to progress toward greater disorder, in accordance with the second law of thermodynamics [22]. In this study, the thermodynamic properties and energy parameters of the 5CPT molecule were computed at the B3LYP/6-311+ +G(d,p) level of theory. The calculated values include vibrational energy (Evib), zero-point energy (ZPE), entropy (S), specific heat capacity at constant volume (C_v), and rotational constants (A, B, and C). These results are summarized in Table 2. The dipole moment of 5CPT was determined to be 5.862 Debye, indicating moderate polarity, a factor that significantly influences molecu-

lar interactions with biological environments, including solubility, membrane permeability, and bioavailability. The calculated zero-point vibrational energy (ZPVE) of 73.83 kcal mol^{-1} suggests a substantial capacity for molecular interactions and internal motion. These relatively high thermodynamic values, interpreted within the framework of the second law of thermodynamics, are essential for thermochemical analysis. They assist in predicting the spontaneity and direction of chemical reactions, thereby underscoring the importance of these findings in assessing the molecular stability and reactivity of 5CPT in biological and pharmaceutical contexts [23].

4.3. Vibrational assignments

Potential energy distributions (PEDs) were obtained using the VEDA program [11], while the fundamental vibrational frequencies of 5CPT were calculated and visualized using GaussView. As a molecule comprising 17 atoms and exhibiting C_1 symmetry, 5CPT displays all 45 expected fundamental vibrational modes. These modes are observed in both the Raman and infrared (IR) spectra. As illustrated in Fig. 3, there is a strong correlation between the theoretically predicted vibrational spectra and the experimental data, with closely matching patterns in both Raman and IR results.

To enhance the correlation between the calculated and experimental vibrational frequencies, a scaling factor of 0.9613 was applied to the computed values [24]. The results of the vibrational analysis, including all observed normal modes along with their corresponding Raman activities and infrared intensities, are presented in Table 3. A detailed discussion of these findings is provided in the subsequent section.

4.3.1. C–H vibrations

The FT-IR and FT-Raman spectra of 5CPT exhibit C–H stretching vibrations within the 3000–3100 cm^{-1} range, characteristic of aromatic systems. C–H in-plane bending vibrations are typically observed between 1300 and 1000 cm^{-1}, while out-of-plane bending vibrations appear in the 1000–750 cm^{-1} region. These spectral regions reflect the molecule's energy absorption patterns and are critical for detailed vibrational analysis. Generally, C–H stretching frequencies in aromatic compounds occur above 3000 cm^{-1}, whereas non-aromatic compounds exhibit

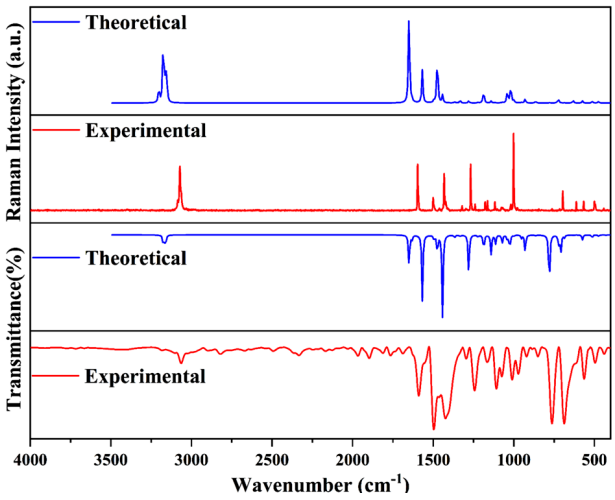

Fig. 3. FT- IR and FT- Raman spectra of 5-chloro-1-phenyl-1H-tetrazole

these vibrations below this threshold–an important distinction for structural characterization [25]. For 5CPT, C–H stretching bands appear at 3065 and 3061 cm^{-1} in the FT-IR spectrum, while corresponding bands are observed at 3070 and 3048 cm^{-1} in the Raman spectrum. Raman bands at 1117, 1030, 1006, and 985 cm^{-1}, along with IR bands at 1100, 1076, and 1011 cm^{-1}, are attributed to C–H in-plane bending vibrations. These experimental findings are in good agreement with the theoretically predicted vibrational modes, further supporting the aromatic nature and vibrational characteristics of the 5CPT molecule.

4.3.2. C–C, C–N, and C–Cl vibrations

Aromatic C–C stretching vibrations typically appear in the 1650–1400 cm^{-1} range [26]. In the case of 5CPT, medium to strong intensity bands were observed at 1549, 1502, and 1428 cm^{-1} in the FT-IR spectrum, and at 1596, 1502, 1430, 1412, and 1380 cm^{-1} in the FT-Raman spectrum. These experimental bands closely align with the theoretically scaled frequencies, which range from 1586 to 1386 cm^{-1}, and show significant potential energy distribution (PED) contributions between 87% and 91%, confirming their assignment to aromatic C–C stretching modes. In addition, ring deformation vibrations were identified at lower wavenumbers, with characteristic bands appearing at 978, 973, 969, 900, 871, and 813 cm^{-1}. These are consistent with the predicted

Table 3. **Vibrational assignments based on PED calculations for 5 chloro-1-phenyl-1H-tetrazole**

S. No	Observed wavenumber (cm^{-1})		Calculated wavenumber (cm^{-1})		IR Intensity (Km mol)	Raman activity (Å^4 amu^{-1})	Assignment with PED (%)
	FT-IR	FT-Raman	Unscaled	Scaled			
1	–	3070 (s)	3202	3079	0	62	νCH (100)
2	3065 (ms)	–	3175	3052	10	259	νCH (99)
3	–	3048 (vw)	3166	3043	7	60	νCH (96)
4	–	–	3158	3035	5	98	νCH (99)
5	3061 (s)	–	3150	3028	0	34	νCH (96)
6	–	1596 (ms)	1650	1586	35	271	νCC (90)
7	1549 (vw)	–	1632	1569	5	6	νCC (89)
8	1502 (vs)	1502 (ms)	1568	1507	70	89	νCC (91)
9	1428 (ms)	1430 (ms)	1495	1437	5	7	νCC (90)
10	–	1412 (vw)	1474	1417	21	134	νCC (88)
11	–	1380 (vw)	1442	1386	87	21	νCC (87)
12	–	1318 (vw)	1367	1314	3	3	νNN (86)
13	1291 (w)	–	1333	1281	1	7	νNN (84)
14	1240 (s)	–	1279	1230	42	5	νNN (85)
15	1164 (ms)	1173 (vw)	1222	1175	2	2	νCN (83)
16	–	1155(vw)	1192	1146	2	7	νCN (82)
17	–	1135 (vw)	1186	1140	15	25	νCN (80)
18	1100 (ms)	–	1141	1097	20	5	bCH (81)
19	1076 (ms)	1117 (vw)	1114	1071	9	1	bCH (79)
20	–	1030 (vw)	1072	1031	9	1	bCH (78)
21	1011 (vw)	1006 (vs)	1040	1000	6	30	bCH (81)
22	–	985 (vw)	1025	986	15	4	bCH (79)
23	–	978 (vw)	1020	980	0	28	Rasymd (77)
24	–	973 (vw)	1015	976	0	12	Rsymd (76)
25	969 (vw)	–	999	961	1	9	Rtrigd (75)
26	–	900 (vw)	952	915	4	1	Rasymd (74)
27	871 (vw)	–	929	893	19	6	Rsymd (73)
28	–	813 (vw)	864	831	1	4	Rtrigd (72)
29	757 (vs)	–	780	750	60	1	νCCl (71)
30	–	705 (vw)	730	702	0	3	bCN (70)
31	–	693 (ms)	722	694	3	6	bCCl (68)
32	683 (ms)	–	709	682	21	0	tRsymd (69)
33	–	655 (vw)	686	660	10	1	‘tRtrigd (67)
34	613 (vw)	–	632	608	0	6	tRasymd (65)
35	552 (ms)	556 (vw)	574	552	5	4	tRsymd (64)
36	489 (vw)	–	514	494	3	4	tRasymd (63)
37	442 (vw)	–	474	456	1	3	ωCCl (62)
38	–	–	425	409	0	0	‘tRtrigd (61)
39	–	–	365	351	1	3	tRasymd (60)
40	–	–	323	310	0	2	ωCH (59)
41	–	–	259	249	1	1	ωCH (57)
42	–	–	255	245	2	2	ωCH (56)
43	–	–	177	170	1	1	ωCH (58)
44	–	–	111	107	1	2	ωCH (55)
45	–	–	43	41	1	4	Butterfly (54)

theoretical values and exhibit PED contributions of approximately 72–77%, further supporting their assignment as ring deformation modes.

In aromatic systems, the C–N stretching vibrations typically occur within the 1200–1000 cm^{-1} range [27]. For the title compound, these modes are iden-

tified by bands at 1164 cm^{-1} in the FT-IR spectrum and at 1173, 1155, and 1135 cm^{-1} in the FT-Raman spectrum. These experimental observations show excellent agreement with the scaled theoretical frequencies at 1175, 1146, and 1140 cm^{-1}. The corresponding potential energy distribution (PED) contributions, ranging from 80% to 83%, further confirm the assignment of these bands to C–N stretching vibrations associated with the tetrazole ring.

C–Cl stretching vibrations typically occur within the 800–600 cm^{-1} range [28]. In the 5CPT molecule, a strong band at 757 cm^{-1} in the FT-IR spectrum is attributed to the C–Cl stretching mode and closely aligns with the scaled theoretical frequency of 750 cm^{-1}, supported by a PED contribution of 71%. This observation confirms the presence of the chlorine substituent on the tetrazole ring. Additionally, minor deformation and torsional modes involving the C–Cl group are observed at lower wavenumbers, including bands at 693 and 442 cm^{-1}.

4.4. Global reactivity parameters and UV-Vis spectral analysis

Frontier molecular orbital (FMO) analysis was conducted to evaluate the chemical and kinetic stability of the 5CPT molecule. FMOs, which represent spatially delocalized molecular orbitals, play a key role in understanding molecular reactivity and interaction potential. The energy gap between the highest occupied molecular orbital (HOMO) and the lowest unoccupied molecular orbital (LUMO) provides critical insight into the molecule's optical, electrical, and chemical properties. In this context, the HOMO acts as an electron donor, while the LUMO serves as an electron acceptor. The HOMO–LUMO energy gap is directly linked to parameters such as molecular hardness, softness, kinetic stability, optical polarizability, and chemical reactivity. A larger gap generally indicates higher kinetic stability and reduced reactivity, whereas a smaller gap implies greater chemical reactivity and increased susceptibility to nucleophilic attack [29]. The intramolecular charge transfer (ICT) behavior within 5CPT is illustrated in the three-dimensional visualization of its FMOs, as shown in Fig. 4, *a*. The calculated HOMO–LUMO energy gap for 5CPT is 5.83 eV, reflecting a stable electronic structure. This value falls within the typical range observed for bioactive compounds, suggesting that 5CPT possesses favorable electronic characteristics for potential biological applications [29]. To further explore the chemical reactivity of 5CPT, several global reactivity descriptors were calculated using Koopmans' theorem. These include ionization potential (I), electron affinity (A), electronegativity (χ), chemical potential (μ), global hardness (η), global softness (S), and the electrophilicity index (ω). The computed results are presented in Table 4. Notably, 5CPT exhibits a global softness of 0.17 eV^{-1} and a corresponding hardness of 2.91 eV, reflecting a moderate balance between stability and reactivity. Compared to hard molecules with wider energy gaps, the relatively soft nature of 5CPT indicates enhanced chemical reactivity and potential for effective interaction with biological targets.

UV-visible spectroscopy is a widely used technique for investigating electronic transitions between molecular orbitals and analyzing the electronic structure of molecules [30]. In the present study, UV spectroscopy was utilized to examine the electronic absorption characteristics of the 5CPT compound. To complement the experimental findings, electronic transitions were also computed using time-dependent density functional theory (TD-DFT). The calculated results, summarized in Table 5, predict three distinct absorption bands at 239.12 nm (5.1850 eV), 231.96 nm (5.3451 eV), and 217.51 nm (5.7001 eV), with corresponding oscillator strengths of 0.0052, 0.1434, and 0.0423, respectively. These transitions are primarily attributed to $\pi \rightarrow \pi^*$ excitations, and the detailed contributions of the individual electronic transitions are also provided in Table 5. The theoretical absorp-

Table 4. **Global reactivity descriptors for 5-chloro-1-phenyl-1H-tetrazole**

Molecular properties	Values by B3LYP/6-311++G(d,p)
HOMO (eV)	–7.54
LUMO (eV)	–1.71
ΔE ($E_{\mathrm{HOMO}} - E_{\mathrm{LUMO}}$) (eV)	5.83
Ionization potential (I) (eV)	7.54
Electron affinity (A) (eV)	1.71
Global hardness (η) (eV)	2.91
Global softness (S) (eV^{-1})	0.17
Electronegativity (χ) (eV)	4.62
Chemical potential (μ) (eV)	–4.62
Global electrophilicity (ω) (eV)	3.67

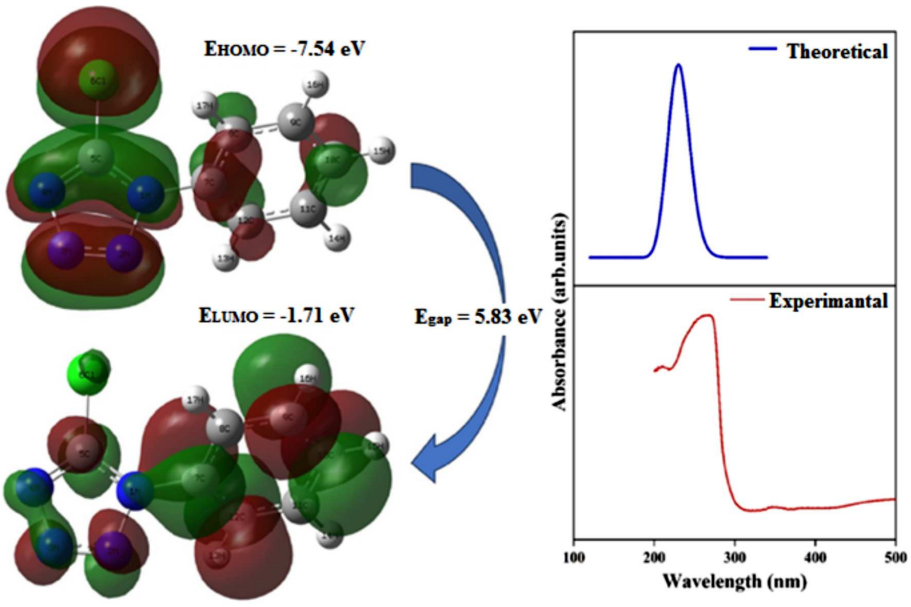

a *b*

Fig. 4. HOMO-LUMO (*a*) and UV-Vis spectrum of 5-chloro-1-phenyl-1H-tetrazole (*b*)

Table 5. **Excited state parameters obtained from TD-DFT/B3LYP/6-311++G(d,p) calculations**

Energy (eV)	Oscillator strength	Computed wavelength (nm)	Experimental wavelength (nm)	Major contributions	Assignment
5.1850	0.0052	239.12	234	H−1 → L (52.60%)	$\pi \rightarrow \pi^*$
5.3451	0.1434	231.96	–	H → L (72.94%)	$\pi \rightarrow \pi^*$
5.7001	0.0423	217.51	–	H−3 → L (48.53%)	$\pi \rightarrow \pi^*$

tion wavelengths are in good agreement with the experimentally observed band at 234 nm, as illustrated in Fig. 4, *b*, further validating the reliability of the TD-DFT approach in modeling the electronic properties of 5CPT.

4.5. MEP and Mulliken atomic charge analysis

Fig. 5 provides two visual representations illustrating the electrostatic and electronic characteristics of the chlorinated tetrazole derivative. Fig. 5, *a* displays the molecular electrostatic potential (MEP) mapped onto the van der Waals surface of the molecule. In this color-coded representation, red regions indicate areas of high electron density (negative potential), while blue regions correspond to areas of low electron density (positive potential) [31]. This gradient effectively highlights potential electrophilic and nucleophilic sites on the molecular surface. The MEP distribution reveals significant electron-rich regions around carbon atoms C5 and C7, as well as nitrogen atoms N2 and N4, suggesting that these atoms may serve as nucleophilic centers in chemical interactions.

Further supporting the MEP analysis, the Mulliken atomic charge distribution calculated at the B3LYP/6-311++G(d,p) level is presented in Fig. 5, *b* and summarized in Table 6. The bar graph highlights atoms with notable negative charges, such as C7 (−0.750), C5 (−0.448), and C10 (−0.344), which correspond closely to the red regions identified on the MEP surface, indicating their potential role as nucleophilic centers [32]. In contrast, hydrogen atoms (H13–H17) exhibit positive charges ranging from +0.162 to +0.194, marking them as electrophilic and electron-deficient, consistent with the blue regions on the MEP map. Notably, the chlorine atom (Cl6) pos-

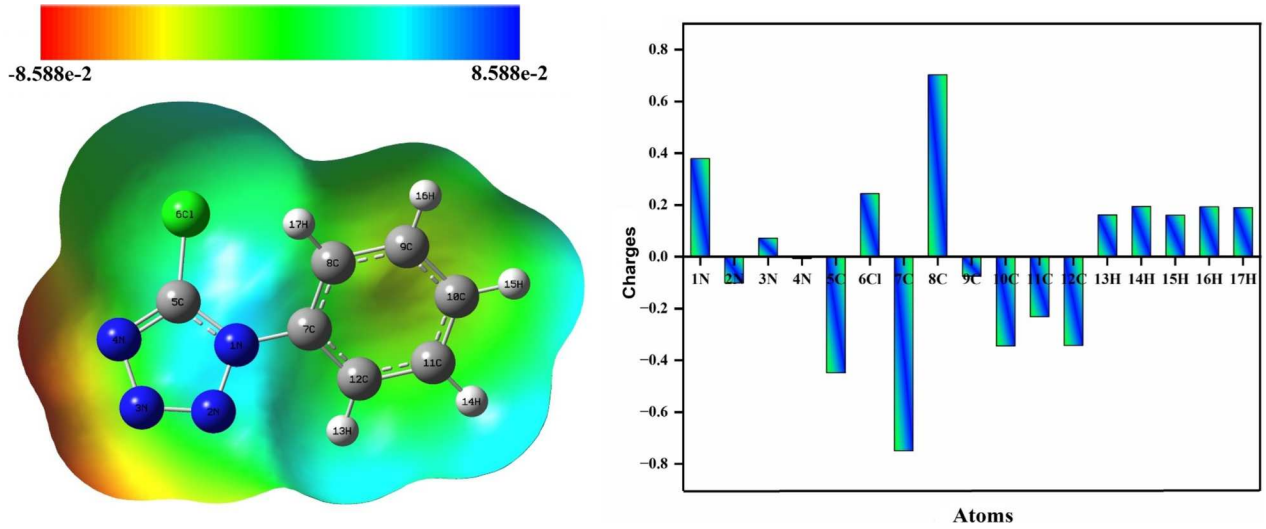

a *b*

Fig. 5. MEP plot (*a*) and Mulliken charge analysis of 5-chloro-1-phenyl-1H-tetrazole (*b*)

sesses a moderately positive charge of +0.244, suggesting a mild electron-attracting character.

4.6. Hirshfeld surface analysis

Hirshfeld surface analysis of the molecule provides deep insight into its intermolecular interactions and molecular geometry. In Fig. 6, *a*, the d_{norm} surface highlights close intermolecular contacts by using a red-white-blue color scheme [33]. Red regions indicate strong and short-range interactions such as hydrogen bonding (typically N–H···O or H···Cl), while blue regions correspond to longer, less significant contacts. The transparent surface overlaid with the molecular structure helps correlate these interaction zones with specific functional groups. Fig. 6, *b* shows the shape index of the molecule, which is useful for identifying π–π stacking interactions. The alternating red and blue patches signify the concave and convex regions, essential for analyzing molecular recognition patterns. Fig. 6, *c* displays the curvedness surface, where green areas indicate relatively flat regions that are commonly involved in π–π stacking or planar contacts, while highly curved regions are shown in blue and red, representing edges and tips of molecular surfaces.

Fig. 6, *d* presents the 2D fingerprint plots, which quantitatively represent all possible intermolecular contacts in the crystal structure. Each plot maps the distances from the Hirshfeld surface to the nearest atom inside (d_i) and outside (d_e) the surface, helping to identify specific interaction types. The fingerprint plots of 5CPT highlight the dominance of N–H interactions, contributing 24.7%, followed by C–H (21.7%) and H–Cl (16.1%) interactions. These interactions are crucial for the stabilization of the crystal lattice and provide a fingerprint unique to the molecular environment. The blue regions in these plots represent areas of high point density, indicating frequent interaction types, while grey areas denote less common interactions. Overall, the combined Hirsh-

Table 6. **Mulliken atomic charges for 5 chloro-1-phenyl-1H-tetrazole**

Atoms	Atomic Charges (Mulliken) by B3LYP/ 6-311++G(d,p)	Atoms	Atomic Charges (Mulliken) by B3LYP/ 6-311++G(d,p)
1N	0.379	10C	–0.344
2N	–0.101	11C	–0.231
3N	0.072	12C	–0.342
4N	–0.006	13H	0.162
5C	–0.448	14H	0.194
6Cl	0.244	15H	0.161
7C	–0.750	16H	0.193
8C	0.703	17H	0.190
9C	–0.075		

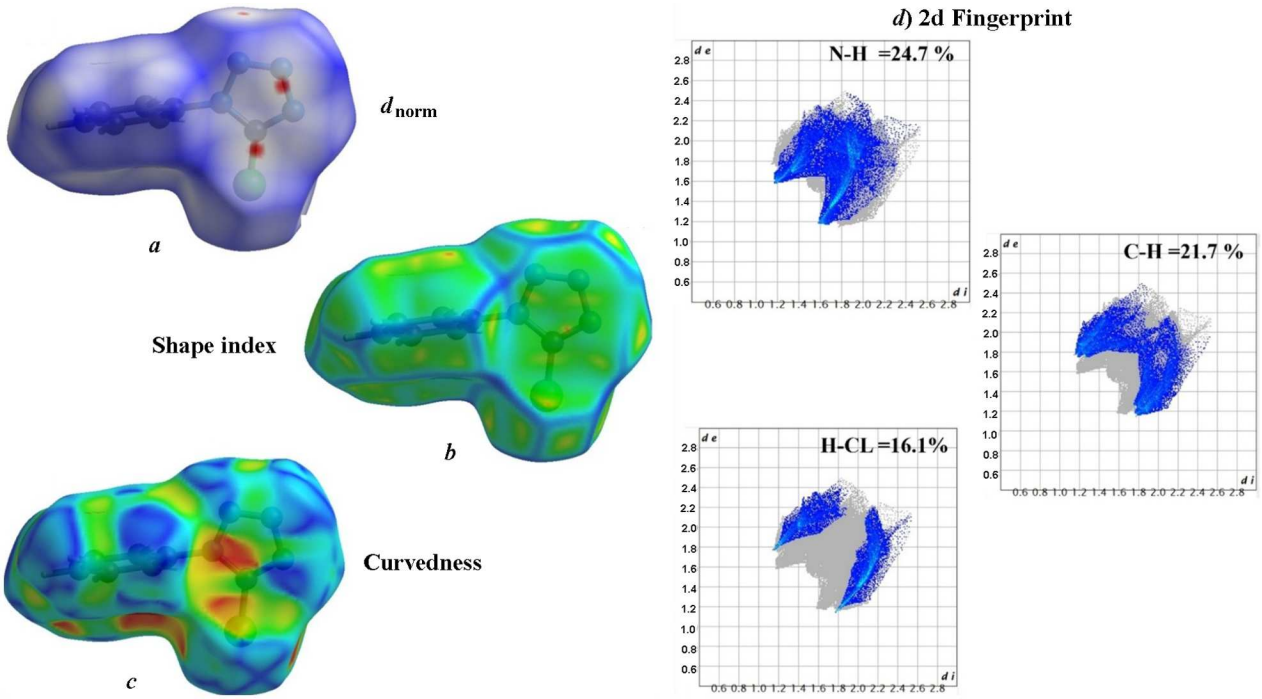

Fig. 6. d_{norm} (*a*), Shape index (*b*), Curvedness (*c*) and 2D Fingerprint plot of 5-chloro-1-phenyl-1H-tetrazole (*d*)

feld surface and fingerprint analysis provides a detailed understanding of the molecular packing, noncovalent interaction patterns, and potential reactive sites within the crystal structure.

4.7. Molecular docking studies

Molecular docking has emerged as a vital tool in modern biological research, particularly in the field of drug discovery, where it aids in identifying potential therapeutic candidates and elucidating specific ligand–protein interactions. This computational approach predicts the most favorable binding orientation of a ligand to a target protein based on minimal binding energy and optimal interaction patterns [34, 35]. In this study, molecular docking simulations were performed to evaluate the interaction of the 5CPT molecule with key breast cancer-related protein targets. These include the human progesterone receptors (PDB IDs: 3D90 and 1ZUC) and the human epidermal growth factor receptor 2 (HER2; PDB ID: 3PP0) [36]. The binding affinities obtained for 5CPT with each of these receptors suggest its potential as a chemotherapeutic agent against breast cancer. The results are summarized in Table 7, which lists the binding energy values for each protein–ligand complex. Fig. 7 visually depicts the docking outcomes, featuring both 2D and 3D interaction diagrams. These illustrations highlight the molecular binding modes of 5CPT, emphasizing key hydrogen bond interactions using color-coded representations of donor and acceptor atoms.

Molecular docking results indicate that 5CPT exhibits its strongest interaction with the HER2 receptor (PDB ID: 3PP0) through a conventional hydrogen bond formed with the GLU A:770 residue at a bond distance of 1.98 Å. The corresponding binding affinity is calculated to be –6.4 kcal/mol, supporting the potential of 5CPT as a therapeutic agent for breast cancer. Additionally, docking analysis with the progesterone receptor (PDB ID: 3D90) reveals that 5CPT forms a single hydrogen bond with the TYR A: 753 residue, exhibiting a bond distance of 2.58 Å and a binding energy of –6.9 kcal/mol, as illustrated in Fig. 7.

Similarly, interaction with another progesterone receptor (PDB ID: 1ZUC) involves a hydrogen bond between 5CPT and the THR A: 829 residue, with a bond length of 1.99 Å and a binding energy of –6.8 kcal/mol. These results, supported by the visual representations in Fig. 7, indicate strong and specific

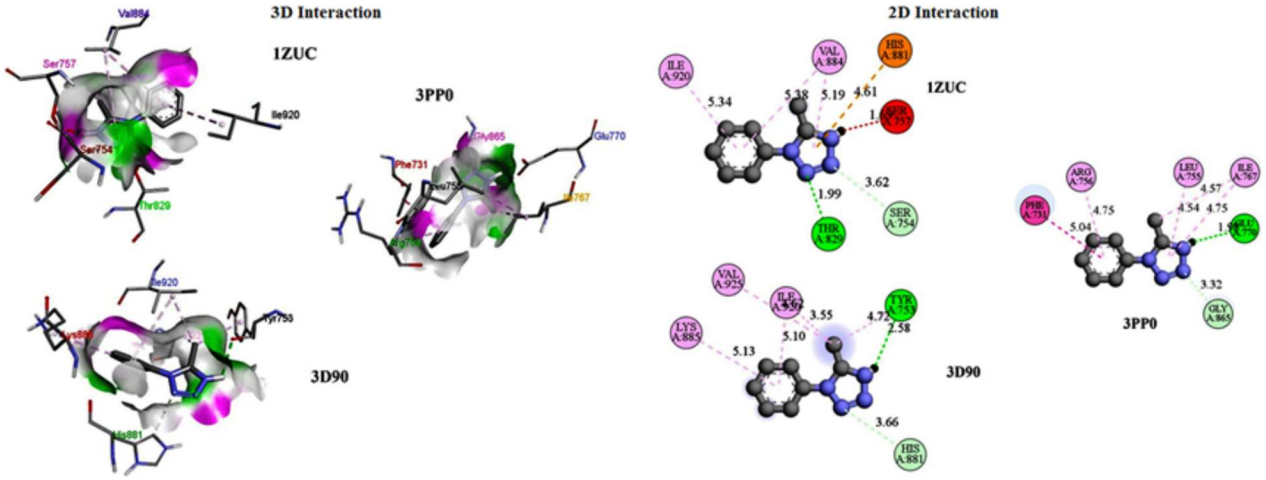

Fig. 7. Molecular docking of 3D and 2D interaction with H-Bond donor-acceptor for 5 chloro-1- phenyl-1H-tetrazole with 1ZUC, 3D90, 3PP0 target proteins

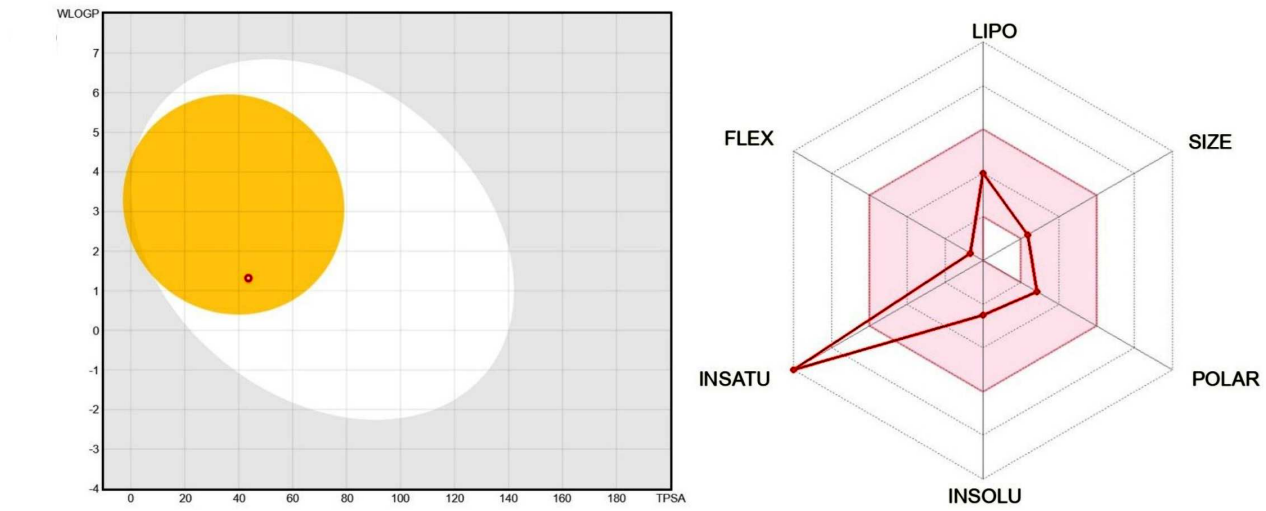

a *b*

Fig. 8. Boiled Egg and (*a*) Radar plot of 5-chloro-1-phenyl-1H-tetrazole (*b*)

Table 7. **Molecular docking binding energy of 5-chloro-1-phenyl-1H-tetrazole**

S. No.	Protein ID	Binding affinity (kcal/mol)	H-bonding involved between ligand and protein	H-bonding distance (Å)
1	1ZUC	–6.8	ILE A: 920, VAL A: 884, HIS A: 881, SER A: 757, SER A: 754, THR A: 829	THR A: 829 (1.99)
2	3D90	–6.9	LYS A: 885, VAL A: 925, ILE A: 926, TYR A: 753, HIS A: 881	TYR A: 753 (2.58)
3	3PP0	–6.4	PHE A: 731, ARG A: 756, LEU A: 755, ILE A: 767, GLU A: 770, GLY A: 865	GLU A: 770 (1.98)

binding of 5CPT to key breast cancer-related proteins, suggesting its potential role in inhibiting their biological functions.

4.8. Pharmacokinetics and Physicochemical Properties

In this study, the metabolic and absorption properties of 5CPT are presented in Table 8. According to the pkCSM server, Caco-2 cell permeability is considered high when the log Papp value exceeds 0.90. Human intestinal absorption (HIA) is considered poor if absorption is below 30%, given the intestine's critical role in nutrient and drug uptake [37]. For 5CPT, the predicted HIA is 89.496%, indicating excellent oral bioavailability. One of the primary challenges in developing topical formulations is overcoming the skin's natural barrier. To evaluate this, several in silico models were employed. The pkCSM results predict a skin permeability (log Kp) value of –2.352 for 5CPT, suggesting strong potential for dermal absorption. The volume of distribution at steady state (VDss) indicates the extent of drug distribution in body tissues relative to plasma. A higher VDss implies broader tissue distribution. For 5CPT, the predicted VDss (log L/kg) is –0.58, suggesting a moderate degree of tissue permeability. The blood–brain barrier (BBB) plays a critical role in preventing neurotoxic compounds from entering the brain. A log BB value greater than 0.3 indicates high permeability, whereas values below –1 suggest limited brain penetration. 5CPT has a log BB of –0.175, reflecting moderate ability to cross the BBB. Central nervous system (CNS) permeability, expressed as log PS, is another important pharmacokinetic parameter. Compounds with log PS <–3 exhibit poor CNS penetration, while those with log PS >–2 are likely to reach the CNS. With a predicted log PS of –1.687, 5CPT demonstrates favorable CNS accessibility. Regarding

Table 8. **ADMET profile of 5-chloro-1-phenyl-1H-tetrazole**

Properties	ADMET Prediction	Value
Absorption	CaCo-2 permeability (log Papp in 10^{-6} cm/s)	1.319
	Intestinal absorption (human) (%)	89.496
	Skin permeability (log Kp)	–2.352
	P-glycoprotein substrate	No
	P-glycoprotein I inhibitor	No
	P-glycoprotein II inhibitor	No
Distribution	VDss (human) (log L/kg)	–0.58
	Fraction unbound (human) (Fu)	0.349
	BBB permeability (log BB)	–0.175
	CNS permeability (log PS)	–1.687
Metabolism	CYP2D6 substrate	No
	CYP3A4 substrate	No
	CYP1A2 inhibitor	Yes
	CYP2C19 inhibitor	No
	CYP2C9 inhibitor	No
	CYP2D6 inhibitor	No
	CYP3A4 inhibitor	No
Excretion	Total clearance (log ml/min/kg)	0.016
	Renal OCT2 substrate	No
Toxicity	AMES toxicity test	No
	Max tolerated dose (human) (log mg/kg/day)	0.742
	hERG I inhibitor	No
	hERG II inhibitor	No
	Oral rat acute toxicity (LD50) (mol/kg)	2.364
	Oral rat chronic toxicity (LOAEL) (log mg/kg_bw/day)	2.326
	Hepatotoxicity	No
	Skin sensitisation	No
	T. *Pyriformis* toxicity (log Bμg/L)	0.628
	Minnow toxicity (log mM)	0.912

Table 9. **Physiochemical properties of 5-chloro-1-phenyl-1H-tetrazole**

Properties	Parameters	Value
Physiochemical properties	Molecular weight (g/mol)	180.59
	No. of H-bond acceptors	3
	No. of H-bond donors	0
	TPSA (Å^2)	43.60
	Fraction Csp^3	0.09
Water Solubility	ESOL	–2.50
	ALI	–2.00
	SILICOS-IT	–2.80
Lipophilicity	iLOGP (log P)	2.01
	XLOGP3 (log P)	1.48
	WLOGP (log P)	1.32
	MLOGP (log P)	1.98
	SILICOS-IT (log P)	1.19
Drug-Likeness	Lipinski	Yes
	Veber	Yes
	Ghose	No
	Egan	Yes
	Bioavailability Score	0.55

excretion, 5CPT is identified as a renal OCT2 substrate and shows a total renal clearance rate of 0.016, based on pkCSM analysis. In terms of toxicity, the predicted oral LD50 in rats is 2.364 mol/kg, and the LOAEL (Lowest Observed Adverse Effect Level) is 2.326 log mg/kg bw/day, suggesting a potential for toxicity at higher doses. Importantly, 5CPT does not inhibit either hERG I or II channels, indicating a low risk of cardiotoxicity and favorable cardiac safety as per pkCSM predictions.

Brain penetration and passive gastrointestinal absorption of 5CPT were further evaluated using the BOILED-Egg predictive model. P-glycoprotein (P-gP), a critical efflux transporter, significantly influences drug bioavailability and clearance through the intestinal, hepatic, and renal systems [38]. The BOILED-Egg model indicates that 5CPT has the ability to cross the blood–brain barrier, as evidenced by its position within the yolk region of the model (Fig. 8, *a*).

5CPT has a molecular weight of 180.59 g/mol and is the only compound among those analyzed to violate the Ghose filter, one of the drug-likeness criteria assessed. The fraction of sp^3-hybridized carbon atoms (Csp^3) in 5CPT is 0.09, suggesting a relatively saturated structure, which is generally linked to enhanced solubility and favorable drug-like properties. The compound's physicochemical characteristics are summarized in Table 9 and visualized in the radar plot shown in Fig. 8, *b*. The predicted lipophilicity values for 5CPT, obtained from different models, are as follows: iLOGP (2.01), XLOGP3 (1.48), WLOGP (1.32), MLOGP (1.98), and SILICOS-IT (1.19), indicating a moderate to high lipophilic nature. Predicted water solubility values derived from ESOL, ALI, and SILICOS-IT models are –2.50, –2.00, and –2.80, respectively, further supporting its acceptable solubility profile. Collectively, these predicted physicochemical and pharmacokinetic properties suggest that 5CPT holds considerable promise as a potential therapeutic agent.

5. Conclusion

In this study, the structural, vibrational, geometrical, docking, and ADMET properties of 5-chloro-1-phenyl-1H-tetrazole (5CPT) were comprehensively analyzed using both theoretical and experimental approaches, including X-ray diffraction (XRD), FT-IR, FT-Raman, and UV-Vis spectroscopy. A strong correlation was observed between the experimental spectroscopic data and the vibrational frequencies obtained from the optimized molecular structure, confirming the reliability of the computational models. The $\pi \rightarrow \pi^*$ electronic transition identified in the UV-Vis spectrum was supported by both theoretical predictions and experimental observations. Molecular orbital analysis revealed a band gap of 5.83 eV, suggesting that 5CPT possesses considerable stability and moderate reactivity. The molecular electrostatic potential (MEP) map further highlighted regions of electrophilic and nucleophilic activity, indicating possible reactive sites within the molecule. Additionally, Mulliken charge analysis provided insights into the charge distribution across the atoms of 5CPT. Using two-dimensional finger maps and the Hirshfeld surface analysis, atom-to-atom interactions in crystal packing modes are described according to their sort and intensity. Molecular docking studies demonstrated strong binding affinities of 5CPT with breast cancer-related protein targets, with binding energies ranging from –6.4 to –6.9 kcal/mol. These results suggest that 5CPT effectively interacts with protein active sites, underscoring its potential as a candidate for breast cancer therapy. Nonetheless, further in vivo and clinical studies are required to confirm its therapeutic efficacy.

The author would like to thank the management of the Kalasalingam Academy of Research and Education for their encouragement and permission to carry out this research.

1. A. Verma, B. Kaur, S. Venugopal, P. Wadhwa, S. Sahu, P. Kaur, D. Kumar, A. Sharma. Tetrazole: A privileged scaffold for the discovery of anticancer agents. *Chem. Biol. Drug. Des.* **100**, 419 (2022).
2. E.A. Popova, A.V. Protas, R.E. Trifonov. Tetrazole derivatives as promising anticancer agents. *Med. Chem.* **17**, 1856 (2017).
3. J. Zhang, S. Wang, Y. Ba, Z. Xu. Tetrazole hybrids with potential anticancer activity. *Eur. J. Med. Chem.* **178**, 341 (2019).
4. W.A. El-Sayed, F.M. Alminderej, M.M. Mounier, E.S. Nossier, S.M. Saleh, A.F. Kassem. Novel 1,2,3-triazole-coumarin hybrid glycosides and their tetrazolyl analogues: Design, anticancer evaluation and molecular docking targeting EGFR, VEGFR-2 and CDK-2. *Mol.* **27**, 2047 (2022).
5. S.K. Gandham, A.A. Kudale, T.R. Allaka, K. Chepuri, A. Jha. New tetrazolopyrrolidine-1,2,3-triazole analogues as potent anticancer agents: design, synthesis and molecular docking studies. *Mol. Divers.***28**, 3313 (2024).

6. A. Mushtaq, R. Asif, W.A. Humayun, M.M. Naseer. Novel isatin–triazole based thiosemicarbazones as potential anticancer agents: synthesis, DFT and molecular docking studies. *RSC* **14**, 14051 (2024).
7. M. Frisch, F. Clemente, M.J. Frisch, G.W. Trucks, H.B. Schlegel, G.E. Scuseria, M.A. Robb, J.R. Cheeseman, G. Scalmani, V. Barone, B. Mennucci, G.A. Petersson, H. Nakatsuji, M. Caricato, X. Li, H.P. Hratchian, A.F. Izmaylov, J. Bloino, G. Zhe. *Gaussian 9* (n.d.).
8. A.D. Becke Density-functional exchange-energy approximation with correct asymptotic behavior. *Phys. Rev. A* **38**, 3098 (1988).
9. C. Lee, W. Yang, R.G. Parr. Development of the Colle-Salvetti correlation-energy formula into a functional of the electron density. *Phys. Rev. B* **37**, 785 (1988).
10. R. Dennington, T. Keith, J. Millam. *GaussView, version 5* (Semichem Inc., 2009).
11. M.H. Jamroz. Vibrational energy distribution analysis VEDA 4 (2004); https://smmg.pl/software/veda/.
12. K. Momma, F. Izumi. VESTA: A three-dimensional visualization system for electronic and structural analysis. *J. Appl. Crystallogr.* **41**, 658 (2008).
13. P.R. Spackman, M.J. Turner, J.J. McKinnon, S.K. Wolff, D.J. Grimwood, D. Jayatilaka, M.A. Spackman. CrystalExplorer: A program for Hirshfeld surface analysis, visualization and quantitative analysis of molecular crystals. *J. Appl. Crystallogr.* **54**, 1006 (2021).
14. O. Trott, A.J. Olson. Software news and update AutoDock Vina: Improving the speed and accuracy of docking with a new scoring function. *J. Comput. Chem.* **31**, 455 (2010).
15. P. Tangyuenyongwatana. Virtual screening for novel 1-deoxy-d-xylulose-5-phosphate reductoisomerase inhibitors: A shape-based search approach. *Virtual screening tool Thai J. Pharmac. Sci. (TJPS)* **41**, (2017).
16. D.S. Biovia. BIOVIA Discovery Studio 2017 R2: A comprehensive predictive science application for the Life Sciences, San Diego, CA, USA http://Accelrys.Com/Products/Collaborative-Science/Biovia-Discovery-Studio (2017).
17. D. E. V. Pires, T. L. Blundell, D. B. Ascher. pkCSM: Predicting small-molecule pharmacokinetic and toxicity properties using graph-based signatures. *J. Med. Chem.* **58,** 4066 (2015).
18. A. Daina, O. Michielin, V. Zoete. SwissADME: A free web tool to evaluate pharmacokinetics, drug-likeness and medicinal chemistry friendliness of small molecules *Sci. Rep.* **7,** 42717 (2017).
19. X.G. Wang, Y. Wang. 5-Chloro-1-phenyl-1H-tetrazole. *Acta Crystallogr. E* **67**, o1633 (2011).
20. V.S. Kunjumol, S. Jeyavijayan, S. Sumathi, N. Karthik. Spectroscopic, computational, cytotoxicity, and docking studies of 6-bromobenzimidazole as anti-breast cancer agent. *J. Mol. Recognit.* **37**, e3074 (2024).
21. J.K. Ojha, G. Ramesh, B.V. Reddy. Structure, chemical reactivity, NBO, MEP analysis and thermodynamic parameters of pentamethyl benzene using DFT study. *Chem. Phys. Impact.* **7**, 100280 (2023).
22. S. Janani, H. Rajagopal, S. Muthu, S. Aayisha, M. Raja. Molecular structure, spectroscopic (FT-IR, FT-Raman, NMR), HOMO-LUMO, chemical reactivity, AIM, ELF, LOL and molecular docking studies on 1-Benzyl-4-(N-Boc-amino)piperidine. *J. Mol. Struct.* **1230**, 129657 (2021).
23. L. Sinha, M. Karabacak, V. Narayan, M. Cinar, O. Prasad. Molecular structure, electronic properties, NLO, NBO analysis and spectroscopic characterization of Gabapentin with experimental (FT-IR and FT-Raman) techniques and quantum chemical calculations *Spectrochim. Acta A Mol. Biomol. Spectrosc.* **109**, 298 (2013).
24. J.P. Merrick, D. Moran, L. Radom. An evaluation of harmonic vibrational frequency scale factors. *J. Phys. Chem. A* **111**, 11683 (2007).
25. S. Sebastian, S. Sylvestre, D. Jayarajan, M. Amalanathan, K. Oudayakumar, T. Gnanapoongothai, T. Jayavarthanan. Molecular structure, normal coordinate analysis, harmonic vibrational frequencies, natural bond orbital, TD-DFT calculations and biological activity analysis of antioxidant drug 7-hydroxycoumarin. *Spectrochim. Acta A Mol. Biomol. Spectrosc.* **101**, 370 (2013).
26. S. Sumathi, S. Jeyavijayan, N. Karthik. Spectroscopic investigations, quantum chemical, molecular docking and drug likeness studies of 3-fluorobenzamide. *J. Sci. Ind. Res.* **83**, 1373 (2024).
27. V.S. Kunjumol, S. Jeyavijayan, N. Karthik, S. Sumathi. Spectroscopic, computational, docking, and cytotoxicity investigations of 5-chloro-2-mercaptobenzimidazole as an anti-breast cancer medication. *Spectrosc. Lett.* **58**, 13 (2024).
28. N. Karthik, S. Jeyavijayan, S. Sumathi. Docking studies, molecular structure, and spectroscopic analysis of 3-chlorobenzamide as an anti-cancer agent. *IJBB* **61**, 204 (2024).
29. A. Jumabaev, B. Khudaykulov, S.-J. Koyambo-konzapa, U. Holikulov, H. Hushvaktov, A. Absanov, I. Doroshenko. Exploring noncovalent interactions of thiophene-2-carboxylic acid in ethanol via vibrational spectroscopy and dft calculations. *Ukr. J. Phys.* **70**, 2071 (2019).
30. V.A. Adole. DFT calculations on three 2,3-dihydrobenzofuran linked chalcones: Structural, HOMO-LUMO and spectroscopic (UV-Vis and IR) interpretation. *J. Chem.* **61**, 147 (2023).
31. A. Jumabaev, H. Hushvaktov, A. Absanov, B. Khudaykulov, Z. Ernazarov, L. Bulavin. Vibrational spectra and computational study of amyl acetate: MEP, AIM, RDG, NCI, ELF and LOL analysis. *Ukr. J. Phys.* **69**, 2071 (2024).
32. V.S. Kunjumol, N. Karthik, S. Sumathi, S. Jeyavijayan. Spectroscopic, computational, docking, and cytotoxicity studies on 5-chlorobenzimidazole as a potent anti-breast cancer agent. *Indian J. Biochem. Biophys.* **61**, 804 (2024).
33. J. Senthil kumar, N. Siva Jyothi, S. Sumathi, N. Karthik, S. Jeyavijayan. Computational, spectroscopic, hirshfeld surface, molecular docking and topological studies on 2-bromo-5- methylpyridine as potent anti-cancer agent. *IJBB* **62**, 683 (2025).

34. J.S. Kumar, N. Karthik, S. Sumathi, N.S. Jyothi, S. Saranya, S. Jeyavijayan. DFT computation, spectroscopic, hirshfeld surface, docking and topological analysis on 2,2,5-trimethyl-1,3-dioxane-5-carboxylic acid as potent anticancer agent. *Int. J. Quantum Chem.* **124**, e27509 (2024).
35. S. Sumathi, S. Jeyavijayan, N. Karthik, A. Karthikeyan, Palani Murugan, V.S. Kunjumol. Molecular structure, spectroscopy, molecular docking and ADMET studies of 2,5-dimethylbenzaldehyde semicarbazone as potent breast cancer agent. *Asian J. Chem.* **36**, 2025 (2024).
36. R. Kalirajan, A. Pandiselvi, B. Gowramma, P. Balachandran, In-silico design, ADMET screening, MM-GBSA binding free energy of some novel isoxazole substituted 9-anilinoacridines as HER2 inhibitors targeting breast cancer. *Curr. Drug Abuse Rev.* **11**, 118 (2019).
37. V.S. Kunjumol, S. Jeyavijayan, N. Karthik, S. Sumathi. Spectroscopic, computational, docking and cytotoxicity studies on 2-(2-chlorophenyl)benzimidazole as a potent anti-breast cancer agent. *Indian J. Pure Appl. Phys.* **62**, 576 (2024).
38. K. AL Azzam. SwissADME and pkCSM webservers predictors: An integrated online platform for accurate and comprehensive predictions for in silico ADME/T properties of artemisinin and its derivatives. *Complex Use of Mineral Resources* **325**, 14 (2022).

Received 20.07.25

Дж.С. Кумар, Н.С. Джіоті,
С. Суматі, Н. Картік, С. Джеявіджаян

ДОСЛІДЖЕННЯ ПОВЕРХНІ ГІРШФЕЛЬДА ТА МОЛЕКУЛЯРНОГО ДОКІНГУ 5-ХЛОРО-1-ФЕНІЛ-1H-ТЕТРАЗОЛУ ЯК ПОТЕНЦІЙНОГО ЗАСОБУ ПРОТИ РАКУ МОЛОЧНОЇ ЗАЛОЗИ

В роботі представлено комплексне теоретичне та спектроскопічне дослідження 5-хлоро-1-феніл-1H-тетразолу (5CPT). Сполуку було охарактеризовано за допомогою методів аналізу ІЧ-Фур'є, КР-Фур'є, рентгенівської дифракції (XRD) та спектроскопії у видимій та ультрафіолетовій областях. Квантово-хімічні розрахунки було виконано на основі методу функціонала густини DFT/B3LYP/6-311++G(d,p) для підтвердження та інтерпретації експериментальних даних. Змодельовану рентгенівську дифрактограму було порівняно з експериментальними даними для структурної валідації. Коливальні частоти, отримані з ІЧ- та КР-спектрів, були розраховані на тому самому теоретичному рівні та показали хорошу відповідність з експериментальними результатами. Для аналізу розподілу електронної густини та ідентифікації реакційноздатних центрів всередині молекули було використано аналіз заселеності за Маллікеном та картування молекулярного електростатичного потенціалу (MEP). Максимуми поглинання в УФ-видимому діапазоні (λ) були визначені як експериментально, так і за допомогою розрахунків на основі теорії функціонала густини, залежного від часу (TD-DFT). Аналіз поверхонь Гіршфельда та діаграм відбитків пальців виявив інформацію про взаємодії всередині молекул та між ними. Крім того, дослідження методом молекулярного докінгу щодо білків, пов'язаних із раком молочної залози, виявили енергію зв'язування в діапазоні від –7,0 до –6,6 ккал/моль. Прогнози ADMET (Absorption-Distribution-Metabolism-Excretion-Toxicity) вказують на сприятливі фармакокінетичні та токсикологічні профілі. У сукупності результати докінгу та ADMET свідчать про те, що 5CPT може бути перспективним кандидатом для розробки препаратів проти раку молочної залози.

Ключові слова: 5-хлор-1-феніл-1H-тетразол, DFT, молекулярний докінг, ADMET (Absorption- Distribution-Metabolism-Excretion-Toxicity), рак молочної залози.